Remote Sensing of Environment 210 (2018) 12–24

Contents lists available at ScienceDirect

Remote Sensing of Environment

journal homepage: www.elsevier.com/locate/rse

Mapping agricultural land abandonment from spatial and temporal segmentation of Landsat time series

He Yin[a,*], Alexander V. Prishchepov[b,c], Tobias Kuemmerle[d,e], Benjamin Bleyhl[d], Johanna Buchner[a], Volker C. Radeloff[a]

[a] SILVIS Lab, Department of Forest and Wildlife Ecology, University of Wisconsin-Madison, 1630 Linden Drive, Madison, WI 53706, USA
[b] Department of Geosciences and Natural Resource Management (IGN), University of Copenhagen, Øster Voldgade 10, DK-1350 København K, Denmark
[c] Institute of Environmental Sciences, Kazan Federal University, Kazan, Tovarisheskaya str. 5, 420097 Kazan, Russia
[d] Geography Department, Humboldt-Universität zu Berlin, Unter den Linden 6, 10099 Berlin, Germany
[e] IRI THESys, Humboldt-Universität zu Berlin, Unter den Linden 6, 10099 Berlin, Germany

ARTICLE INFO

Keywords:
Change detection
Agricultural land abandonment
Landsat
Land-use change
Land-cover probability
Segmentation
LandTrendr
Trajectory-based approach
Europe
Caucasus

ABSTRACT

Agricultural land abandonment is a common land-use change, making the accurate mapping of both location and timing when agricultural land abandonment occurred important to understand its environmental and social outcomes. However, it is challenging to distinguish agricultural abandonment from transitional classes such as fallow land at high spatial resolutions due to the complexity of change process. To date, no robust approach exists to detect when agricultural land abandonment occurred based on 30-m Landsat images. Our goal here was to develop a new approach to detect the extent and the exact timing of agricultural land abandonment using spatial and temporal segments derived from Landsat time series. We tested our approach for one Landsat footprint in the Caucasus, covering parts of Russia and Georgia, where agricultural land abandonment is widespread. First, we generated agricultural land image objects from multi-date Landsat imagery using a multi-resolution segmentation approach. Second, we estimated the probability for each object that agricultural land was used each year based on Landsat temporal-spectral metrics and a random forest model. Third, we applied temporal segmentation of the resulting agricultural land probability time series to identify change classes and detect when abandonment occurred. We found that our approach was able to accurately separate agricultural abandonment from active agricultural lands, fallow land, and re-cultivation. Our spatial and temporal segmentation approach captured the changes at the object level well (overall mapping accuracy = 97 ± 1%), and performed substantially better than pixel-level change detection (overall accuracy = 82 ± 3%). We found strong spatial and temporal variations in agricultural land abandonment rates in our study area, likely a consequence of regional wars after the collapse of the Soviet Union. In summary, the combination of spatial and temporal segmentation approaches of time-series is a robust method to track agricultural land abandonment and may be relevant for other land-use changes as well.

1. Introduction

Land-use and land-cover change is one of the main drivers of global change (Lambin and Geist, 2006). Growing food demand has triggered rapid agricultural expansion and the loss of forest, grassland and wetland (Meyer and Turner, 1992; Ramankutty and Foley, 1999). However, agricultural land abandonment also is a common land-use change process in many parts of the world as a result of trade, socio-economic shocks, institutional structures and land-use policies (Gellrich et al., 2007; Haddaway et al., 2014; Meyfroidt et al., 2016; Müller et al., 2009).

Agricultural land abandonment has manifold effects on both human society and ecosystems. Abandonment can have negative effects on food security and local livelihoods (Khanal and Watanabe, 2006; Knoke et al., 2013), may threaten farmland biodiversity (Beilin et al., 2014; Obrist et al., 2011), and the persistence of cultural landscapes (Van Eetvelde and Antrop, 2004). Yet, agricultural land abandonment is also an opportunity for ecological restoration (Haddaway et al., 2014; Plieninger et al., 2014), forest regeneration on abandoned fields enhances carbon sequestration (Kuemmerle et al., 2011; Schierhorn et al., 2013) and it benefits woodland birds and large mammal populations (Blondel et al., 2010; Sieber et al., 2015). Many of these effects vary

* Corresponding author.
E-mail address: hyin39@wisc.edu (H. Yin).

https://doi.org/10.1016/j.rse.2018.02.050
Received 25 August 2017; Received in revised form 28 January 2018; Accepted 22 February 2018
0034-4257/ © 2018 Elsevier Inc. All rights reserved.

depending on the time since abandonment. For example, below-ground carbon sequestration is five times larger in the first 20 years after abandonment than thereafter, whereas above-ground sequestration increases dramatically after 5-10 years of abandonment in the temperate region (Goulden et al., 2011; Kurganova et al., 2014; Schierhorn et al., 2013). To better understand and evaluate the diverse social and ecological consequences of abandonment, it is, therefore, necessary to assess the exact timing of agricultural land abandonment.

Although monitoring agricultural land abandonment is a priority for many national agricultural monitoring programs (Keenleyside and Tucker, 2010; Renwick et al., 2013), consistent maps of abandoned agricultural lands, and robust approaches for generating such maps from satellite data, are lacking. Agricultural land abandonment is defined as agricultural land that has not been used for a minimum of two to five years (FAO, 2016; Pointereau et al., 2008). It is necessary to distinguish long-term fallow (abandoned) from temporal fallow fields, which are a part of the crop rotation cycle. It might be particularly important in multi-year crop rotation systems, where the crop rotation includes prolonged fallow periods (Loboda et al., 2017). Moreover, the trajectory of abandonment is often not uniform over time (Kraemer et al., 2015). Temporal re-cultivation may occur a few years after an agricultural field was abandoned if land-use policies or other socio-economic settings such as the fluctuation of wheat prices changed (Meyfroidt et al., 2016; Smaliychuk et al., 2016). All this contributes to difficulties in accurately monitoring agricultural land abandonment with Earth Observation products.

The freely accessible Landsat archive provides great opportunity to map agricultural dynamics due to the availability of imagery dating back to the 1970s (Loveland and Dwyer, 2012; Wulder et al., 2012). The medium resolution of Landsat imagery makes it suitable to monitor changes in agriculture fields (Duveiller and Defourny, 2010; Ozdogan and Woodcock, 2006). Previously, Landsat imagery has been used to monitor agriculture expansion (Carlson et al., 2012; Gibbs et al., 2010) and intensification (Kuemmerle et al., 2013; Lasanta and Vicente-Serrano, 2012), estimate yields (Lobell et al., 2015; Rudorff and Batista, 1991), identify crop types (Schultz et al., 2015; Zheng et al., 2015) and delineate field boundaries (Evans et al., 2002; Yan and Roy, 2014). However, the use of Landsat time series for agricultural monitoring is still under development, even though the value of time series has been highlighted in coarser-scale MODIS based mapping of agriculture and abandonment (Alcantara et al., 2012; Estel et al., 2015).

Landsat image time series are increasingly used to monitor land-use and land cover change on an annual basis and many trajectory-based approaches have emerged (Huang et al., 2010; Kennedy et al., 2010; Verbesselt et al., 2010; Zhu and Woodcock, 2014). Trajectory-based approaches make full use of image time series to identify the breakpoints and temporal segments that represent land cover change, for example, for forest monitoring (DeVries et al., 2015; Grogan et al., 2015). However, it is not clear how well these methods are suited to map land use change processes, such as agricultural land abandonment at Landsat scale.

The analysis of time series imagery has focused on pixel-level algorithms. The drawback of pixel-based approaches is that they can generate noisy outputs, because spectral reflectance at single-pixel level is more prone to problems related to misregistration or errors in the cloud and shadow screening (Blaschke and Strobl, 2015; Yu et al., 2016). Furthermore, agricultural land abandonment is typically a management decision at the field level, and it is best to combine spatial, spectral and temporal information to produce annual cropland maps from the full Landsat archive (Schmidt et al. 2016). Mapping agricultural land abandonment at object-level, such as agricultural plots, could thus take advantages of spatial dependencies and reduce mapping uncertainties at the pixel-level. However, spatial segmentation used for change detection is typically based on only a pair of imagery before and after the change (Desclée et al., 2006; Duveiller et al., 2008), and the temporal information that is inherent in the full-time series has not been fully utilized. It may be beneficial to incorporate both spatial and temporal segmentation to understand the dynamics of land-use systems, such as agricultural abandonment (Dutrieux et al., 2016; Gómez et al., 2011).

Our overall goal was to develop and test a new methodology that captures agricultural land abandonment by combining a spatial and temporal segmentation. Our objectives were to separate agricultural land abandonment from active agriculture, temporary fallow and recently re-cultivated abandoned land, and to identify the timing of changes using long-term remote sensing time-series Landsat imagery. Using FAO's (2016) definition, we considered agricultural land abandonment as agricultural land that has not been used for at least five years. Abandoned land that was re-used for more than four years was defined as re-cultivated. Our manuscript is organized as follows. First, we introduce our study area, followed by our tests to how to segment multi-date Landsat imagery spatially. Next, we describe our maps of agricultural land abandonment at both object- and pixel- level from agricultural land probability time series using a temporal segmentation approach (LandTrendr, Kennedy et al., 2010) and compare their mapping accuracies. Last, we discuss our findings and their implications for future research and land management.

2. Study area

We mapped agricultural land abandonment for one Landsat footprint path 170/row 030, World Reference System (WRS)-2 (Fig. 1). Landsat 170/030 covers parts of Georgia and the North Caucasian Federal District of Russia including the Chechen Republic, the Republic of Ingushetia, the Republic of North Ossetia-Alania, the Republic of Kabardino-Balkaria, Stavropolskij Kraj.

The two most common soils, Chernozems and Gleysols, and particularly Chernozems in the study site are well-suited for crop production. Precipitation ranges from 347 mm in the lowlands to 1677 mm in the mountains (Afonin et al., 2008). The accumulated heat beneficial to plant growth over 5 °C varies from zero GDD (growing degree days) in the mountains to 4,038 GDD in the lowlands (Afonin et al., 2008). Winter crops dominate crop production, primarily winter wheat in the southern foothills of the Caucasus Mountains. Livestock production, dairy farming, pork and poultry production are also common (ROSSTAT, 2016).

After the breakup of the Soviet Union in 1991, agricultural land in Russia was privatized and redistributed in land shares among former employees of state and collective farms (Lerman et al., 2004). In the north Caucasus republics (Chechnya, Dagestan, Ingushetia, Kabardino-Balkaria, and North Ossetia), however, land privatization of former collective and state farms was not allowed (Uzun et al., 2014), and the Soviet farm structure (average farm size > 100 ha) was largely retained (Hartvigsen, 2014; Uzun et al., 2014). Several armed conflicts occurred in the region and shaped land use (O'Loughlin and Witmer, 2011). According to official statistics, there was widespread agricultural land abandonment in the study area. In our study site, sown areas declined by 17% from 1990 to 2010 compared to the 1990 level and livestock declined by 40% (ROSSTAT, 2016), which indicates considerable cropland and managed grassland abandonment (Ioffe et al., 2004).

3. Data and methods

We mapped agricultural land abandonment using Landsat imagery from 1985 to 2015 using both spatial and temporal segmentation (Fig. 2). First, we applied multi-resolution spatial segmentation in eCognition™ (Baatz and Schäpe, 2000) to create spatially homogenous objects based on multi-date cloud-free Landsat imagery (Section 3.2). Second, we estimated the agricultural land probability for each object by summarizing per-pixel probability estimated from a random forest model based on annual Landsat spectral-temporal metrics (Section 3.3.1). Third, we applied a temporal segmentation algorithm,

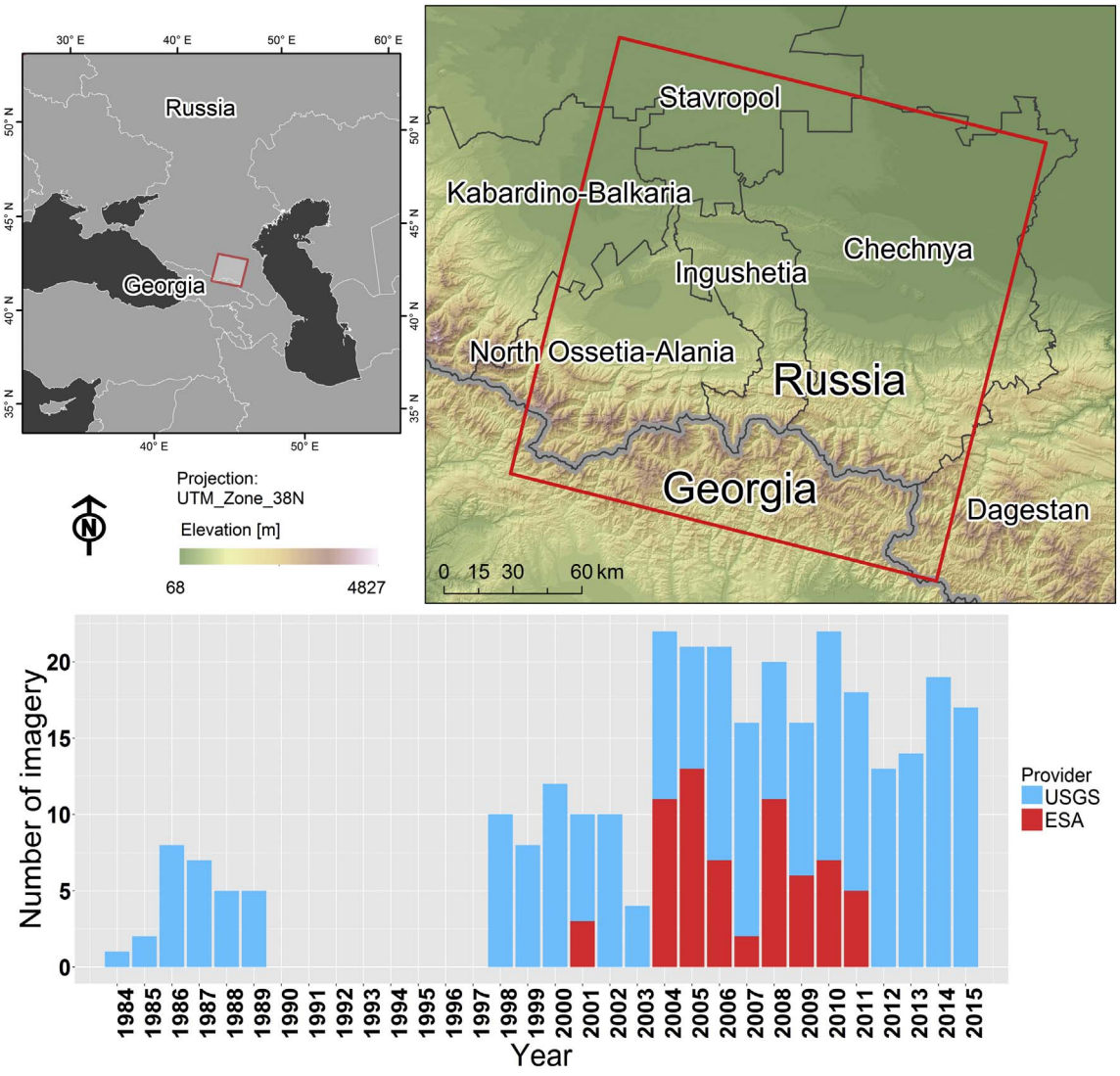

Fig. 1. Location of the study area and the numbers of the Landsat imagery used for the agricultural land abandonment mapping. The Landsat footprint (path/row 170/030) is outlined in red. (For interpretation of the references to color in this figure legend, the reader is referred to the web version of this article.)

LandTrendr (Kennedy et al., 2010), on the agricultural land probability time series to create temporal segments at the object-level (Section 3.3.2). We classified agricultural land abandonment, stable agricultural land, fallow and re-cultivation based on the temporal segments, and identified the first and the last year of the change. Fourth, we validated our agricultural land abandonment map using a disproportional sampling approach (Section 3.3.3) and compared it with a conventional pixel-level mapping approach (Section 3.4). Fifth, we estimated the total area of agricultural land abandonment using error-adjusted stratified estimation as described in Olofsson et al. (2014).

3.1. Landsat pre-processing

We downloaded all the available geo-rectified L1T Landsat imagery less than 70% cloud cover for the study area. For the years with few L1T imagery, we added three L1G images acquired between April and October with less than 10% cloud cover. In total, we obtained 236 and 65 images from the United States Geological Survey (USGS) and the European Space Agency (ESA), respectively (Fig. 1, Fig. S1).

To ensure consistency among different sensors and dates, we performed atmospheric correction and radiometric calibration using the Landsat Ecosystem Disturbance Adaptive Processing System (LEDAPS) for each USGS and ESA Landsat image (Masek et al., 2006). Additionally, we applied FMASK to mask cloud, cloud shadows and snow for each image (Zhu and Woodcock, 2012). We co-registered all the L1G archives to the L1T images using automated tie point matching with less than half a pixel (15 m) in positional error (Exelis Visual Information Solutions, 2014).

3.2. Agricultural land object generation

We stacked cloud-free L1T imagery acquired on 31 August 1989, 17 September 1998, 21 May 2007 and 30 July 2015 as input layers for the spatial segmentation because multi-temporal data create temporally homogenous objects (Desclée et al., 2006; Dutrieux et al., 2016).

We used a bottom-up multi-resolution segmentation algorithm in eCognition™ (Baatz and Schäpe, 2000). This approach initiates each pixel as a single segment and merges spatially adjacent segments based on their similarity until the desired scale is met. Scale is a 'window of perception' and determined by the spatial resolution of the satellite imagery and the size of the objects of interest (Marceau, 1999). Specifically, the scale parameter defines the maximum standard deviation of heterogeneity used for image segmentation (Benz et al., 2004). A higher scale value allows more tolerance of heterogeneity within one object and results in larger image objects (Fig. S2). The merging decision is based on local homogeneity criteria which describes the

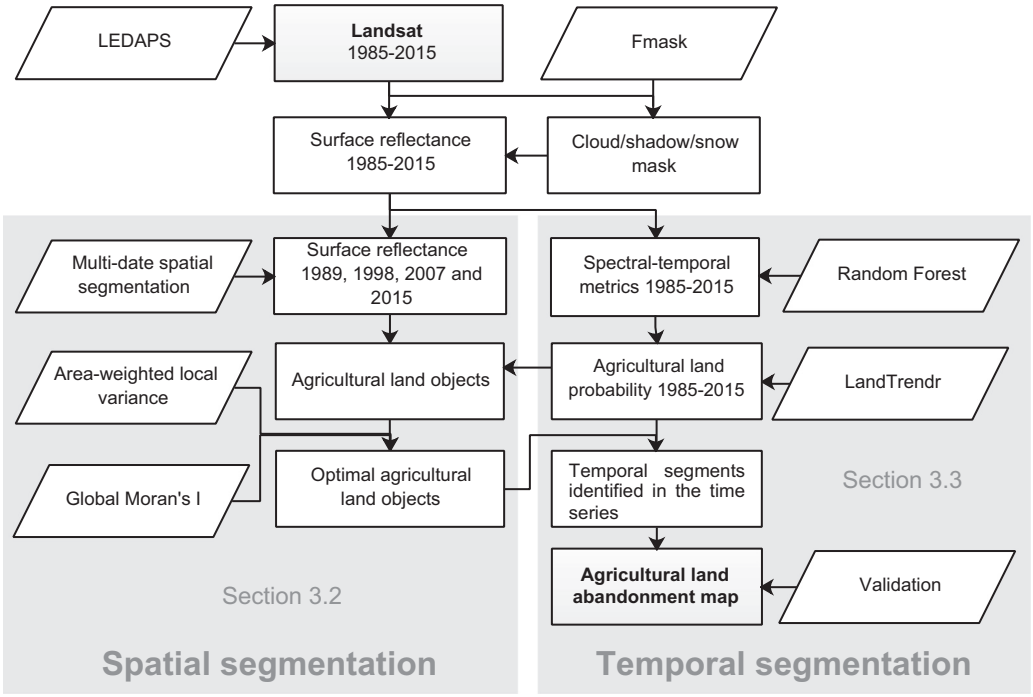

Fig. 2. Flowchart of spatial and temporal segmentation.

similarity (e.g. Euclidean distance) of adjacent objects. Two homogeneity criteria, spectral and shape homogeneity are used in eCognition™. The spectral criterion is more important for generating better segmentation (Yu et al., 2016). However, a certain degree of shape homogeneity often improves the quality of object extraction because it ensures the compactness of spatial objects (eCognition, 2011). We assigned equal weight to each band and used weights for color and shape of 0.8 and 0.2, respectively (Pu et al., 2011; Yu et al., 2016).

Applying single-scale parameter to different types of land-cover that vary in size often consolidates small neighboring objects into larger ones (under-segmentation), or partitions single large objects into smaller sub-objects (over-segmentation) (Evans et al., 2002). The conventional evaluation approach requires to check for either visually, and test different parameters iteratively, which is time-consuming and subjective (Vieira et al., 2012). Spatial variance and autocorrelation provide alternative means to assess segmentation quality because optimal segmentation should minimize intra-segment variance while maximizing inter-segment difference (Espindola et al., 2006; Johnson and Xie, 2011). We parameterized the segmentation model following Johnson & Xie (2011). First, we generated multiple segmentations using different scale parameters. Second, we calculated area-weighted local variance (*ALV*) and Global Moran's I (*MI*) of layers for each segmentation. Because we were only interested in the accuracy of agricultural land segmentation, *ALV* (Eq. (1)) and *MI* (Eqs. (2) and (3)) were only calculated for the agricultural land, which was mapped from multi-temporal image stack and a random forest classifier (Section 3.3.1). Third, we calculated the value Global Score (*GS*) (Eq. (4)), which combines intra-segment variance and inter-segment autocorrelation.

$$ALV = \frac{\sum_{j=1}^{m}((\sum_{i=1}^{n} v_{i,j} * a_{i,j}) / \sum_{i=1}^{n} a_{i,j})}{m} \quad (1)$$

where $a_{i,j}$ and $v_{i,j}$ are area and spectral variance of object i in the layer j, n and m stand for the number of object and input layers.

$$MI = \frac{\sum_{k=1}^{m} I_k}{m} \quad (2)$$

$$I = \frac{n * \sum_{i=1}^{n}\sum_{j=1}^{n} w_{i,j}(s_i - \bar{s}) * (s_j - \bar{s})}{\left(\sum_{i=1}^{n}\sum_{j=1}^{n} w_{i,j}\right) * \sum_{i=1}^{n}(s_i - \bar{s})} \quad (3)$$

where I_k is Global Moran's I for the input layer k, $w_{i,j}$ is equal to spatial weight between object i and j with values of 0 (non-adjacent) and 1 (adjacent), s_i and $\bar{s}$ are aggregate spectral reflectance of the object i and the whole layer.

$$GS = ALV_{norm} + I_{norm} \quad (4)$$

where ALV_{norm} and I_{norm} stand for normalized area-weighted local variance (*ALV*) and Global Moran's I (*I*), respectively.

We identified optimal image segmentation scale as the one with the lowest value of Global Score.

3.3. Agricultural land abandonment mapping

3.3.1. Agricultural land probability estimate

We used spectral-temporal metrics derived from Landsat imagery as input variables to estimate the per-pixel agricultural land-cover probability for each year (Yin et al., 2017). Agricultural land included managed cropland and managed grasslands, i.e., pastures and hay fields. To reduce classification error due to data scarcity, we included ± 1 year imagery around the target years, which allowed us to calculate spectral-temporal metrics for each year except 2003 because there were too few clear observations (Fig. S1). We calculated five metrics for each reflectance band: the mean, median, standard deviation, 25th percentile, and 75th percentile for each year.

We analyzed both Landsat imagery and high-resolution images from Google Earth to collect training samples. First, we selected Landsat pixel-size samples. Second, these samples were labeled as active and non-active agriculture fields using high-resolution imagery available via Google Earth™ mapping platform (Fig. S3). Third, we visually examined and updated the label of each training sample for each year. We excluded samples that were not active agricultural land based on our visual interpretation of Landsat and ASTER imagery. Active agriculture is typically tilled, which means, there is a clear soil signal, and a drop of NDVI during the growing season. Furthermore, active agriculture land has a smoother spatial texture and homogenous vegetation growth

within a field (Fig. S4). We analyzed approximately 3000 Landsat pixel-size training samples, of which 1500 were active agriculture land.

We estimated pixel-wise probabilities for both active agricultural and non-agricultural land using the random forest model implemented in the statistical software CRAN R (R Core Team, 2016) for each year from 1985 to 2015. The number of variables randomly sampled as candidates at each split (*mtry*) was set to the square root of the number of input variables, and the minimum size of the terminal nodes was set to 10. Per-pixel class probability was estimated based on the percentage of tree votes for a given class. Per-pixel agricultural land probability was aggregated by object using the median value.

To examine the robustness of the random forest model, we calculated the F1 score for agricultural land using the out-of-bag (OOB) error provided in the random forest model. For each random forest models during 1985 and 2015, we increased the number of the tress from 1 to 1000 at a step of 1. The F1 score was calculated as $F1 = 2 \times UA \times PA / (UA + PA)$, where UA and PA stand for user's and producer's accuracy derived from the out-of-bag (OOB) error in random forest model, respectively. The result showed that the F1 score was higher than 90% using a tree number of 1000 for every year from1985 to 2015 (Fig. S5). We, therefore, used a tree number of 1000 to train the random forest model for each year.

We generated an agricultural land mask for our study area using annual agricultural land probability from 1985 to1989. First, we converted the continuous agricultural probabilities to discrete land-cover classes. We labeled objects as agricultural lands when the agricultural land probability was larger than non-agricultural land probability. Second, we summarized the frequency of agricultural land between 1985 and 1989. Third, we mapped objects as agricultural land when objects were considered as an agricultural area in more than three of the five years between 1985 and 1989.

3.3.2. Temporal segmentation and agricultural land abandonment labeling

We used a temporal segmentation approach LandTrendr to detect changes in each object class probability over time (Fig. 3). LandTrendr decomposes annual Landsat time series into different segments to capture both long-term gradual and short-term drastic changes. The core curve fitting function used in LandTrendr is MPFIT, which is an implementation of the Levenberg-Marquardt algorithm (Markwardt, 2009). The MPFIT is used to solve non-linear least squares problems and is an efficient and robust optimizer for a variety of fitting functions (Kennedy et al., 2007; Vrieling et al., 2017).

We used several metrics to describe temporal segments in the time series of agriculture land probability, including the start and end time and segment duration (in years). Because of the Landsat data gap in the early 1990s, we ran LandTrendr on agriculture land probability from 1998 to 2015.

Based on the fitted agriculture land probability time series, we distinguished agricultural land abandonment, re-cultivation, and fallow from stable agricultural land (Fig. 3). First, we labeled those pixels as abandoned that changed from active agricultural land (agricultural probability value ≥ 0.5) to non-active agricultural land (agricultural probability value < 0.5) and for which the duration of the non-active period was longer than five years. The timing of agricultural land abandonment was recorded correspondingly. We calculated agricultural land abandonment follows:

$$LA = 1 \text{ if } (v_1 \geq 0.5)\&(v_2 < 0.5)\&(d > 5)\&[(v_2 + m) < 0.5] \quad (5)$$

where LA is agricultural land abandonment, v_1 and v_2 are pre-change-vertex and post-change-vertex values for focal segment, respectively, d is the post-change-segment duration and m is the post-change-segment magnitude.

If the agricultural land was not active from 1998 to 2003, we considered the corresponding object as agricultural land abandonment before or in 1998 (hereafter 1998). Second, we labeled agricultural land abandonment objects that were converted to active agricultural land and remained active for more than four years as re-cultivation. Third, agricultural land that stayed inactive for less than five years was mapped as fallow land. Last, agriculture objects which were never labeled as abandoned, re-cultivation, or fallow were mapped as stable agricultural land.

3.3.3. Validation of agricultural land abandonment map

We calculated confusion matrices and producer's, user's, and overall accuracies to address the accuracy of the agricultural land abandonment map, accounting for possible sampling bias (Card, 1982). To avoid problems with small sample sizes for rare thematic classes such as agricultural land abandonment, we used disproportionate stratified sampling at the pixel level for validation (Olofsson et al., 2014; Stehman et al., 2003). We randomly selected 150 Landsat pixels within the stable agricultural land and non-agricultural land classes, and 75 pixels within each change class as reference samples following

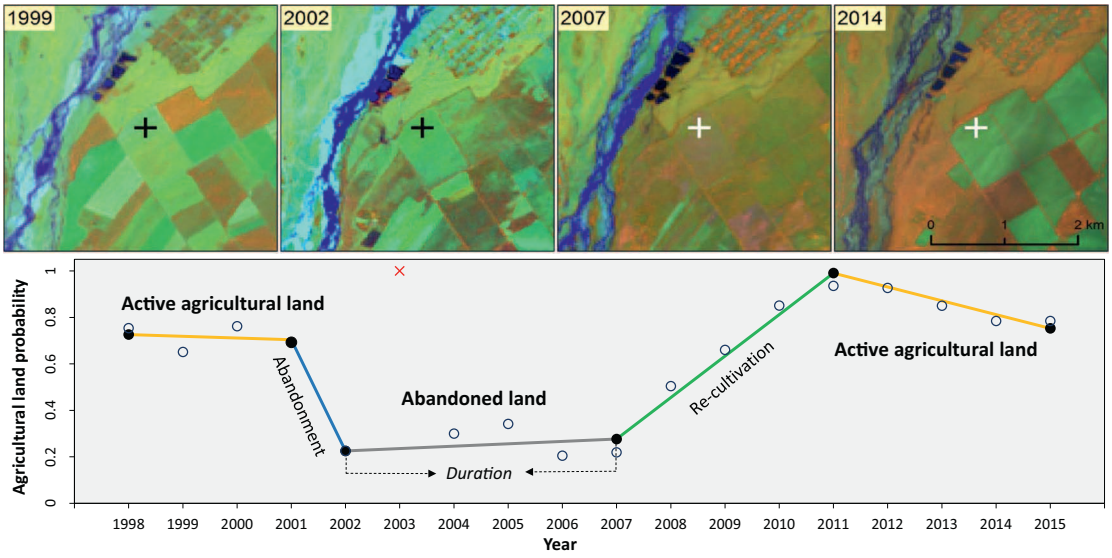

Fig. 3. Example of a temporal segmentation with related Landsat imagery (RGB: NIR, SWIR 1, Red), for the pixel indicated by either a black or white crosshair. Blue circles in the plot indicate Landsat derived agriculture land probability. Black dots show vertices of fitted segments. Fitted segments are shown by the lines and each color of lines refers to a certain process. Data gap is indicated by a red cross. (For interpretation of the references to color in this figure legend, the reader is referred to the web version of this article.)

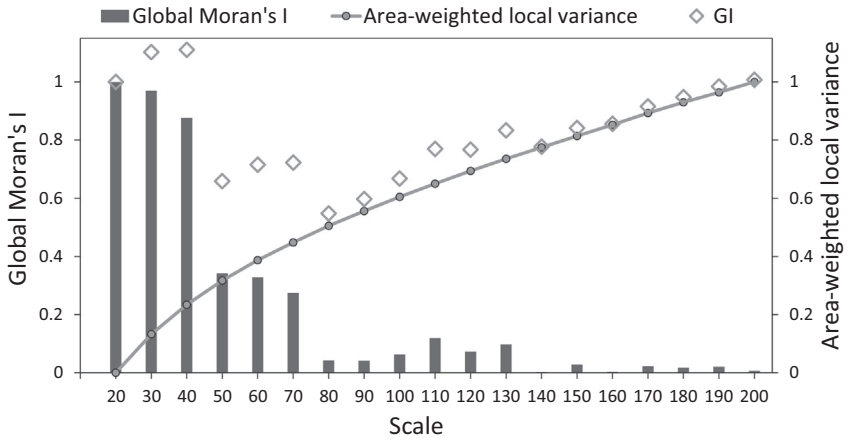

Fig. 4. Area-weighted local variance (ALV), Global Moran's I (MI) and Global Score (GS) as a function of segmentation scale.

Congalton and Green (2009). The actual land cover change was assessed based on visual interpretation of the remote sensing time series (Cohen et al., 2010; Estel et al., 2015). Each sample was labeled without knowledge of the mapped class label using the Landsat time series from 1985 to 2015 and 56 L1T ASTER imagery acquired from 2001 to 2015. To avoid misinterpretation due to intra-annual variability of crop growth, we selected cloud-free imagery acquired in spring (May–June), summer (July–August) and autumn (September–October) for interpretation. High-resolution imagery from Google Earth and Bing Aerial maps aided our visual interpretation. In addition, we examined temporal profiles of the MODIS NDVI time series (MOD13Q1) to support labeling samples with data gaps in ASTER, Landsat, Google Earth and Bing Aerial images. We used the time series visual interpretation tool HUB TimeSeriesViewer (Jakimow et al., 2017) for this task.

3.4. Pixel-level agricultural land abandonment mapping and comparison

We compared the object-based with the pixel-based agricultural land abandonment map. In addition to creating temporal segments at the object-level, we ran LandTrendr on agriculture probability time series per-pixel and labeled agricultural land abandonment, re-cultivation, fallow and stable agricultural land following the same labeling approach as described in the Section 3.3.2.

We estimated mapping accuracy of pixel-based agricultural land abandonment map using the same validation samples generated from the object-based map (Section 3.3.3). Because the strata (i.e. map class) of the object-based abandonment map were different from the pixel-based abandonment map, the inclusion probability of validation samples needed to be taken into account to derive unbiased estimators (Stehman, 2014). We calculated the inclusion probability-adjusted overall, producer's and user's accuracy for the pixel-based agricultural land abandonment map and compared them with estimators derived from the object-based map.

For stratum i, the agreement between map class ($\hat{e}_i$) and reference class (e_i) was defined as y_i.

$$y_i = \begin{cases} 1 & if\ \hat{e}_i = e_i \\ 0 & if\ \hat{e}_i \neq e_i \end{cases} \quad (6)$$

Overall accuracy (OA) was calculated as the sample mean of agreement ($\overline{y}_h$) between the map class (pixel-based agricultural land abandonment map) and the reference class weighted by the inclusion probability (ω_h) in each stratum h (object-based agricultural land abandonment map):

$$OA = \sum_{h=1}^{n} \omega_h * \overline{y}_h \quad (7)$$

where the inclusion probability ω_h was calculated as the area proportion of stratum h. User's accuracy (UA) and producer's accuracy (PA) for a map class c (e.g. agricultural land abandonment, stable cropland) were calculated as:

$$UA_c = \left(\sum_{h=1}^{n} N_h * \overline{y}_h\right) / \left(\sum_{h=1}^{n} N_h * \overline{x}_h\right) \quad (8)$$

$$PA_c = \left(\sum_{h=1}^{n} N_h * \overline{y}_h\right) / \left(\sum_{h=1}^{n} N_h * \overline{z}_h\right) \quad (9)$$

where N_h is the population size for stratum h, $\overline{y}_h$ is the sample mean of agreement between map class (pixel-based agricultural land abandonment map) and reference class in each stratum h for map class. $\overline{x}_h$ and $\overline{z}_h$ were calculated as the sample proportion of map class c and reference class c in each stratum h, respectively.

4. Results

4.1. Spatial segmentation

Our spatial segmentation captured the boundaries of fields well, but both intra- and inter-segment variances changed considerably when we changed the scale parameters (Fig. 4). Area-weighted local variance within segments gradually increased as the segmentation scale parameter increased, but the inter-segment variance (global Moran's I) drastically decreased. There was no substantial difference in Moran's I autocorrelation when scale parameters were > 70. To avoid including different land-use trajectories into the same object, we used a scale of 50 to obtain actual field size and create homogenous agricultural land objects.

Visual inspection of our resulting multi-resolution segmentation confirmed that image objects captured patterns on the ground well, both in the parts of the study area where fields were large and homogenous (Fig. 5B) and where they were more fragmented resulting in heterogeneous agricultural landscapes (Fig. 5A,C). Regardless of field size, shape, and orientation, the agriculture land objects matched well with actual field boundaries, although some big fields were subdivided into a few smaller objects (Fig. 5B).

4.2. Agricultural land abandonment mapping

We found strong cross-boundary differences in agricultural land abandonment in our study site (Fig. 6). Chechnya and Ingushetia had much higher agricultural land abandonment rates (24.6% and 21.0%, respectively) than the other three administrative regions. In Chechnya, marginal lands especially areas close to the Caucasus Mountains were

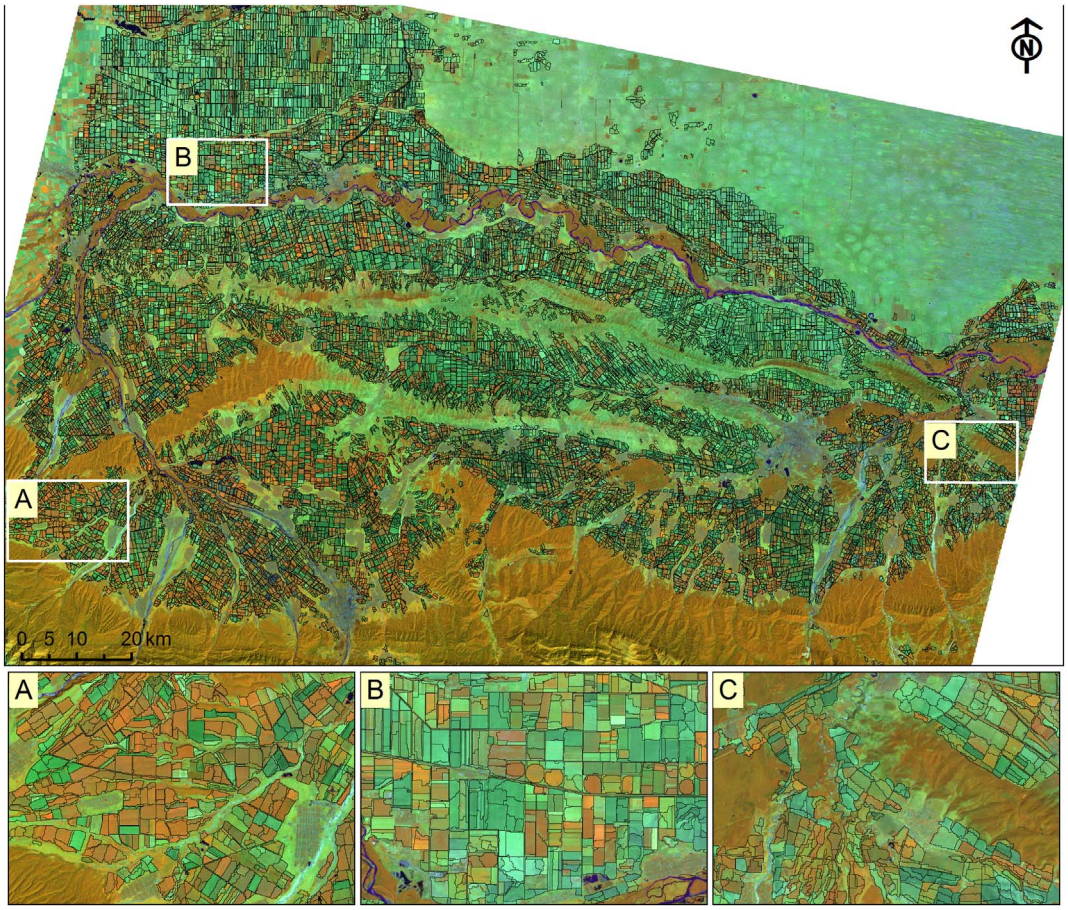

Fig. 5. Agricultural land objects overlaid on one Landsat image (31 Aug 1989 shown as RGB = NIR, SWIR 1, Red) for the majority of the study area, and for three subsets.

more likely to be abandoned. Stavropolskij Kraj and Kabardino-Balkaria had the least agricultural land abandonment (1.4% and 3.4%). Regions with higher agricultural land abandonment rates also had lower re-cultivation rates (10.3% and 39.4% in Ingushetia and Stavropolskij Kraj respectively).

4.2.1. Agricultural land abandonment mapping accuracy

Our spatial and temporal segmentation and subsequent classification resulted in an accurate map of abandonment. The overall mapping accuracy of our agricultural land abandonment map was 97 ± 1%, albeit with variations in accuracy among classes. Stable classes, such as stable agricultural land and non-agricultural land, had producer's and user's accuracies ranging from 95% to 99% (Fig. 7). Agricultural land abandonment classes, however, showed a somewhat lower mapping accuracy with an average producer's and user's accuracy of 69% and 66%, respectively. Compared to agricultural land abandonment classes, re-cultivation generally had a lower mapping accuracy.

Confusions between different abandonment classes, i.e., false assignment of the year when abandonment occurred, was the main reason for the lower mapping accuracy for the agricultural land abandonment classes (Table 1). Relaxing the precision of timing of agricultural land abandonment resulted in higher mapping accuracies of change classes, e.g., producer's and user's accuracies increased by 10–40 percentage points when ± 2 year mapping precision was deemed sufficient (Fig. S6).

4.2.2. Pixel-based mapping and comparison

The spatial pattern of agricultural land abandonment maps illustrated the advantages of using objects as mapping units (Fig. 6). Comparing the pixel-based and object-based maps showed more small, isolated land-cover-change patches and a large variation within fields for the pixel-based approach. On marginal areas that were far from core agricultural lands, the pixel-based map confused agricultural land abandonment with non-agriculture land (Fig. 6, subsets 1, 2). Similarly, in heterogeneous landscapes, such as areas close to settlements, the pixel-based approach classified mixed vegetation and impervious pixels as agricultural land abandonment or stable agriculture land (Fig. 6, subset 3).

Mapping accuracies were consistently lower for the pixel-based classes compared to the object-based map (Fig. 7). The overall accuracy of the pixel-based map was 82 ± 3%, but this was largely due to the stable classes, which cover about 80% of the study region. The average producer's and user's mapping accuracies of the agricultural land abandonment map classes in the pixel-based map were only 18% and 10%, respectively. Compared to the object-based agricultural land abandonment map, there was much higher confusion between agricultural land abandonment and stable agricultural land (Table 2).

5. Discussion

Agricultural land abandonment is difficult to detect because agricultural land abandonment is a heterogeneous land use change process and it can result in a range of post-abandonment land cover types. However, accurate information about the timing and extent of agricultural land abandonment is crucial, for instance, to investigate the drivers of agricultural land abandonment, to estimate carbon sequestration, and to see the economic and environmental costs of potential re-cultivation. In Russia, the latter is particularly important given the rising interest of the Russian Government in re-cultivation of some abandoned lands, and elsewhere, given EU policy programs to maintain

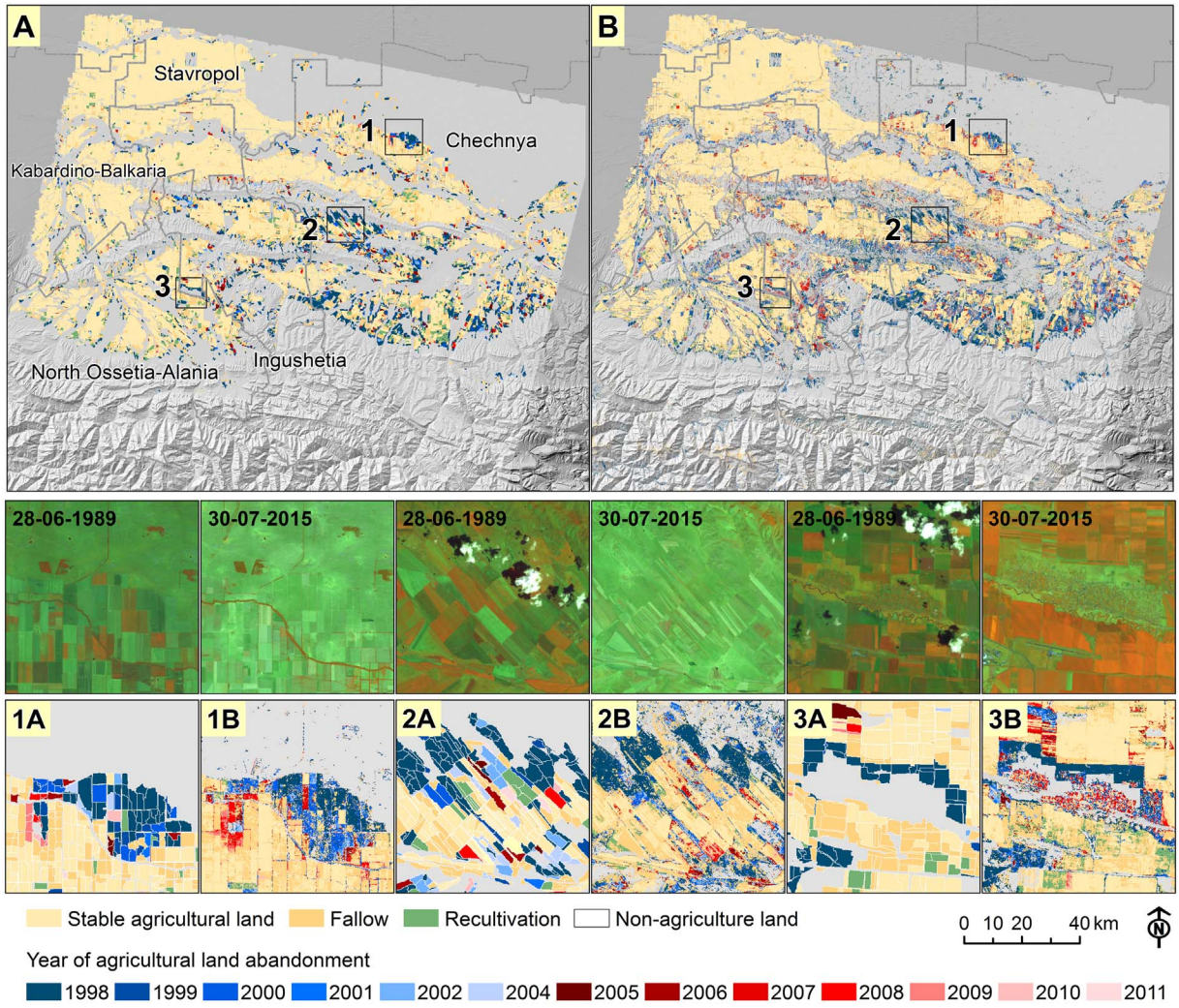

Fig. 6. Object-level (A) and pixel-level (B) agricultural land abandonment map with three subsets and related Landsat imagery (RGB: NIR, SWIR 1, Red). (For interpretation of the references to color in this figure legend, the reader is referred to the web version of this article.)

farming on socio-economically and agro-environmentally marginal lands (Shagaida et al., 2017). We were able to map the spatial and temporal patterns of agricultural abandonment accurately by combining spatial and temporal segmentation of a time series of Landsat data. Our results showed that spatial and temporal segmentation could improve the mapping of agricultural land abandonment and accurately capture both the extent and the year of agricultural land abandonment based on 30-m Landsat imagery.

5.1. Spatial segmentation

Spatial segmentation based on textural features and neighborhood information that is inherent in temporal stacks of Landsat imagery allowed us to create spatial objects that served as a suitable unit for agriculture change monitoring. Compared to pixel-based mapping, agricultural land change detection at object-level achieved substantially higher overall mapping accuracy (overall accuracy: 97 ± 1% vs. 82 ± 3%) and much higher detection probability of agricultural land abandonment (Fig. 7). We see the main advantages of the object-based detection of agricultural land abandonment as follow: 1) by averaging out of the heterogeneity within agricultural fields we created maps of fields, which are the units at which management decisions are made (Fig. 6, subset 1), 2) by removing the “salt and pepper effect” due to individual pixels or small patches we avoided misclassification of agricultural land abandonment in non-agricultural areas (Fig. 6, subset 2), and 3) spatial segmentation reduced confusions in a heterogeneous environment such as urban areas, where mixed pixels are prevalent (Fig. 6, subset 3).

We used a multi-resolution segmentation approach to generate agriculture objects, and we achieved reliable results (Figs. 4,5). To identify the optimal spatial segmentation, we used the Global Score calculated from the area-weighted local variance and Global Moran's I accounting for the intra-segment variance and inter-segment difference. The overall performance was strong, but in some cases large fields were split into smaller ones. The reason was that boundaries of an agricultural landscape were relatively stable while the cropping pattern within fields changed (Blaschke and Strobl, 2015). We were not concerned about this though, because our goal was not to extract field boundaries (as in Yan and Roy 2016). Instead, our focus was to group pixels that have similar spatiotemporal characters (Dutrieux et al., 2016). If the goal were to identify actual agricultural fields and associated changes, further refinement would be necessary to reduce under- and over-segmentation (Johnson and Xie, 2011).

5.2. Temporal segmentation

One of the great advantages of Landsat data is that the availability of consistent data for over three decades, which allowed us to analyze a time series and apply temporal segmentation to map agricultural land abandonment. Temporal segmentation, such as entailed in LandTrendr,

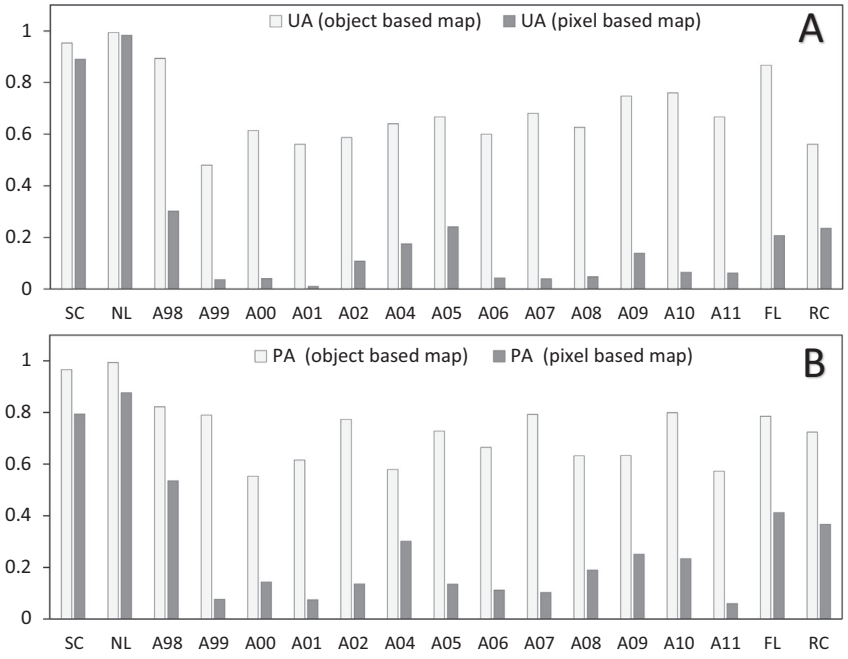

Fig. 7. Comparison of producer's (A) and user's accuracy (B) of our object- and pixel-based agricultural land abandonment maps. SA: stable agricultural land, NL: non-agricultural land, A: agricultural land abandonment (i.e. A11 indicates agricultural land abandonment in 2011), FL: fallow, RC: re-cultivation.

can greatly improve forest change monitoring. Here, we applied LandTrendr to monitor agriculture change. We successfully separated agricultural land abandonment from other agricultural land use change such as fallow and re-cultivation. Compared to multi-date agricultural land abandonment mapping based on few time-steps (Kraemer et al., 2015; Kuemmerle et al., 2008; Prishchepov et al., 2012), the Landsat time series allowed us to map both gradual changes and abrupt deviations in land-cover. Being able to do so is particularly important when monitoring land-use classes with high inter-annual and intra-annual variability such as agriculture. Furthermore, the temporal segmentation allowed us to label the timing of agricultural land abandonment well, which is important when assessing the ecological consequence of abandonment (Deng et al., 2013; Navarro and Pereira, 2015) and designing land use policies (Renwick et al., 2013; Swinnen et al., 2017).

Although we achieved a relatively high mapping accuracy, there were still a few uncertainties. Mapping accuracy increased substantially when temporal mapping precision was relaxed to ± 2 years (Fig. S6), indicating class confusion regarding the timing of abandonment. Confusion often exists between change classes in neighboring years when a trajectory-based approach for mapping changes at annual intervals is used (Grogan et al., 2015; Kennedy et al., 2012).

The spectral and phenological similarity between agricultural land and other herbaceous classes was another error source. Compared to forest and non-forest land, which have distinctive spectral reflectances, the spectral boundary between agriculture, especially low-intensive agricultural lands, and natural herbaceous classes, is less distinct (Xian et al., 2009). The data paucity and irregular temporal coverage of Landsat imagery further added difficulties in separating active and non-active agriculture lands for some areas. With the availability of Landsat

Table 1
Error matrix of our object-based land abandonment map (area proportion in percent). Years refer to the year when abandonment first occurred. SA: stable agricultural land, NL: non-agriculture land, FL: fallow, RC: re-cultivation.

	Reference																
	SA	NL	1998	1999	2000	2001	2002	2004	2005	2006	2007	2008	2009	2010	2011	FL	RC
SA	**16.171**															0.792	
NL	0.490	**73.016**															
1998		0.140	**1.872**	0.028												0.028	0.028
1999		0.018	0.111	**0.222**	0.043	0.012	0.006		0.012	0.006						0.018	0.012
2000		0.002	0.014	0.011	**0.073**	0.008	0.003	0.002	0.002	0.003	0.002						
2001		0.002	0.009	0.003	0.003	**0.037**	0.008	0.002	0.001	0.001			0.001				
2002		0.006	0.018	0.006	0.009		**0.133**	0.018	0.009	0.003		0.003	0.003			0.012	0.006
2004		0.001	0.002	0.005			0.001	**0.060**	0.009	0.004	0.004		0.001		0.001	0.002	0.002
2005		0.000	0.008	0.002			0.002	0.006	**0.103**	0.019	0.002	0.006	0.006				
2006	0.002	0.003	0.014	0.003	0.002		0.003	0.002	0.005	**0.077**	0.007	0.005	0.002		0.002	0.002	
2007		0.002	0.010		0.001		0.001	0.001		0.002	**0.059**	0.005	0.002	0.001	0.001		
2008	0.001	0.001	0.003	0.001		0.003	0.002	0.000	0.001		0.001	**0.041**	0.009	0.002	0.001	0.001	
2009			0.002					0.001				0.005	**0.045**	0.005	0.001	0.001	0.001
2010	0.001				0.001					0.001			0.001	**0.034**	0.007	0.001	
2011			0.001				0.001	0.001			0.000		0.001	0.001	**0.017**	0.004	
FL	0.067	0.269	0.202													**4.369**	0.134
RC	0.011		0.011				0.011	0.011								0.333	**0.482**
	Overall accuracy: 97 ± 1%																

Table 2
Error matrix of pixel-based land abandonment map (area proportion in percent). Years refer to the year when abandonment first occurred. SA: stable agricultural land, NL: non-agriculture land, FL: fallow, RC: re-cultivation.

	Reference																
	SA	NL	1998	1999	2000	2001	2002	2004	2005	2006	2007	2008	2009	2010	2011	FL	RC
SA	**13.394**	0.007	0.061				0.007	0.003			0.004	0.001	0.002	0.005	0.002	1.481	13.394
NL	0.339	**64.268**	0.225	0.015	0.008	0.002	0.013	0.004			0.002		0.004	0.001	0.002	0.504	0.339
1998	0.226	2.594	**1.296**	0.033	0.008	0.008	0.012	0.002	0.007	0.004	0.002	0.004	0.002	0.001	0.001	0.072	0.226
1999		0.003	0.199	**0.020**	0.084	0.076	0.005	0.003	0.002	0.002	0.001		0.001			0.145	
2000		0.497	0.109	0.043	**0.029**	0.003	0.010	0.005		0.002	0.003	0.001	0.002	0.002	0.000		
2001		0.569	0.087	0.013	0.016	**0.009**	0.019	0.003	0.007	0.004		0.001	0.002		0.001	0.156	
2002			0.076	0.013	0.009	0.001	**0.025**	0.008	0.006	0.010	0.001	0.002	0.001	0.001	0.001	0.072	
2004			0.002	0.017	0.003	0.001	0.011	**0.027**	0.010	0.007	0.002			0.001		0.072	
2005			0.004	0.007		0.010	0.003	0.009	**0.020**	0.011	0.001	0.005	0.001				
2006		0.002	0.007	0.008		0.002	0.011	0.020	0.029	**0.014**	0.007	0.001	0.006		0.001	0.219	
2007		0.003	0.032	0.001	0.004	0.002	0.006	0.007	0.019	0.016	**0.007**	0.001	0.003	0.001	0.002	0.079	
2008			0.032	0.013		0.001	0.003	0.004	0.017	0.016	0.002	**0.012**	0.003	0.001	0.000	0.144	
2009			0.003		0.002			0.003	0.006	0.010	0.006	0.010	**0.018**	0.003	0.001	0.072	
2010	0.113				0.002	0.002		0.001	0.003	0.005	0.004	0.005	0.010	**0.010**	0.002	0.001	0.113
2011	0.001		0.001				0.003		0.002	0.002	0.004	0.005	0.005	0.004	**0.002**		0.001
FL	2.561	4.910	0.262	0.064	0.031	0.009	0.036	0.015	0.023	0.020	0.023	0.009	0.019	0.017	0.015	**2.174**	2.561
RC	0.226	0.490			0.007	0.002	0.012		0.001	0.002						0.091	**0.226**
	Overall accuracy: 82 ± 3%																

8 and Sentinel-2 imagery, and new products such as the Harmonized Landsat Sentinel-2 data (HLS, https://hls.gsfc.nasa.gov), these mapping uncertainties could be reduced substantially.

5.3. Method transferability

We tested our approach in one Landsat footprint where agricultural land abandonment was widespread. The study site represented a large gradient with agricultural land abandonment in the lowland steppes, where abandonment resulted in herbaceous vegetation communities, and in the foothills of the Caucasus Mountains, where shrub and tree encroachment followed abandonment. It suggests that our method might be transferred to map agricultural land abandonment in other parts of Europe and the world with similar land-use change processes. Adjustment, however, may be needed before directly applying our approach to other areas where social and physical environments are different. First, our approach can be easily adapted to different definitions of agricultural land abandonment. Depending on local climate-soil conditions or agrarian policies, the fallow period can be longer than five years (García-Ruiz and Lana-Renault, 2011; Pointereau et al., 2008). In this study, we used FAO's agricultural land abandonment definition (agricultural land set aside at least for a five-year period), which fits the Caucasus region reasonably well (Gasanov et al., 2013; Ioffe and Nefedova, 2004; Saraykin et al., 2017). Second, spatial segmentation may need to consider field boundary changes. For example, many former Soviet countries broke up large-scale collective farms into small-scale private household plots and thus created cropland fragmentation (Davis, 1997; Hartvigsen, 2014). To avoid grouping pixels with different land-use trajectories into one object, the imagery used for segmentation should include images before and after the field boundary change. Third, pixel or sub-pixel analysis is preferred if changes occur in fields that are around or smaller than a pixel (Jain et al., 2013). In many developing countries, small-scale agriculture is prevalent, and pixel-based methods may advantageous. Our approach may also be applicable for other land-use change studies especially for mapping land-use changes that occur in aggregated patches, such as forest disturbances (Coops et al., 2010; Gómez et al., 2011), wetland dynamics (Dronova et al., 2011) and urban sprawl (Xie and Weng, 2016). To map complex land cover classes, new classification approaches, such as dimensionality reduction techniques of Landsat time series has the potential to archive better classification result (Yan and Roy, 2015).

5.4. Agricultural land abandonment in the Caucasus

Agricultural land abandonment was widespread throughout Eastern Europe after the collapse of socialism (Alcántara et al., 2013), but the rate of abandonment varied greatly (Kraemer et al., 2015; Kuemmerle et al., 2009; Müller and Munroe, 2008; Prishchepov et al., 2012). In comparison, we observed relatively low rates of abandonment. We found about 12.0% of agricultural land was abandoned in the North Caucasus during 1989–2015, considerably less than the 31% in European Russia but similar to Belarus (13.0%) (Prishchepov et al., 2017), and higher than in Armenia and Azerbaijan (4.9%) (Baumann et al., 2015). Reasons for this difference may have been both relatively good soil quality and population growth in the North Caucasus. Contrary to other regions of Russia, Chechnya was the region with the highest population growth rate of 15% from 2002 to 2010 (ROSSTAT, 2010).

We found strong cross-boundary differences in agricultural land abandonment rates, most likely due to political, institutional of socio-economic factors (Fig. 6). Specifically, we found the highest agricultural land abandonment rates in Chechnya (24.6%) and Ingushetia (21.0%) where the long lasting and brutal Chechen Wars took place after the dissolution of the Soviet Union. The considerable amount of agricultural land abandonment was likely caused by these wars (O'Loughlin and Witmer, 2011).

6. Conclusion

We successful mapped agricultural abandonment by combining spatial and temporal segmentation. We included all available Landsat imagery in our analyses in order to distinguish stable, abandoned and fallow agricultural land, as well as re-cultivated abandoned land. Our accuracy assessment of the object-based map confirmed the reliability of our approach, which is transferable to map agricultural land abandonment elsewhere and to the classification of other land-use change classes. Our results show that most of the agricultural land abandonment in the North Caucasus occurred before 2000 and were concentrated where armed conflicts occurred (e.g., Chechnya and Ingushetia). Ultimately, our new approach for satellite-based agricultural monitoring can thus lead to a deeper understanding of land-use and land-cover change.

Acknowledgements

We gratefully acknowledge support for this research by the Land-Cover and Land-Use Change (LCLUC) Program of the National Aeronautic Space Administration (NASA) through Grant NNX15AD93G. We thank R. Kennedy for providing LandTrendr codes, B. Jakimow for providing the HUB TimeSeriesViewer tool and the OpenLab initiative under the Russian Government Program of Competitive Growth of Kazan Federal University. We also thank S. Stehman for his suggestions on accuracy assessment and appreciate constructive comments from two anonymous reviewers.

Appendix A. Supplementary data

Supplementary data to this article can be found online at https://doi.org/10.1016/j.rse.2018.02.050.

References

Afonin, A.N., Greene, S.L., Dzyubenko, N.I., Frolov, A.N., 2008. Interactive agricultural ecological atlas of russia and neighboring countries. In: Economic Plants and their Diseases [WWW Document], . http://www.agroatlas.ru.

Alcantara, C., Kuemmerle, T., Prishchepov, A.V., Radeloff, V.C., 2012. Mapping abandoned agriculture with multi-temporal MODIS satellite data. Remote Sens. Environ. 124, 334–347. http://dx.doi.org/10.1016/j.rse.2012.05.019.

Alcántara, C., Kuemmerle, T., Baumann, M., Bragina, E.V., Griffiths, P., Hostert, P., et al., 2013. Mapping the extent of abandoned farmland in Central and Eastern Europe using MODIS time series satellite data. Environ. Res. Lett. 8, 35035. http://dx.doi.org/10.1088/1748-9326/8/3/035035.

Baatz, M., Schäpe, A., 2000. Multiresolution Segmentation-an optimIzation Approach for High Quality Multi-scale Image Segmentation. Angew. Geogr. Info. Verarbeitung. ichmann-Verlag, Heidelberg, pp. 12–23.

Baumann, M., Radeloff, V.C., Avedian, V., Kuemmerle, T., 2015. Land-use change in the Caucasus during and after the Nagorno-Karabakh conflict. Reg. Environ. Chang. 15, 1703–1716. http://dx.doi.org/10.1007/s10113-014-0728-3.

Beilin, R., Lindborg, R., Stenseke, M., Pereira, H.M., Llausàs, A., Slätmo, E., et al., 2014. Analysing how drivers of agricultural land abandonment affect biodiversity and cultural landscapes using case studies from Scandinavia, Iberia and Oceania. Land Use Policy 36, 60–72. http://dx.doi.org/10.1016/j.landusepol.2013.07.003.

Benz, U.C., Hofmann, P., Willhauck, G., Lingenfelder, I., Heynen, M., 2004. Multi-resolution, object-oriented fuzzy analysis of remote sensing data for GIS-ready information. ISPRS J. Photogramm. Remote Sens. 58, 239–258. http://dx.doi.org/10.1016/j.isprsjprs.2003.10.002.

Blaschke, T., Strobl, J., 2015. What's wrong with pixels? Some recent developments interfacing remote sensing and GIS. Interfacing Remote Sens. GIS 1–7.

Blondel, J., Aronson, J., Bodiou, J.-Y., G., B., 2010. The Mediterranean Region Biological Diversity in Space and Time. Oxford University Press, New York.

Card, D.H., 1982. Using known map category marginal frequencies to improve estimates of thematic map accuracy. Photogramm. Eng. Remote. Sens. 48, 431–439.

Carlson, K.M., Curran, L.M., Ratnasari, D., Pittman, a.M., Soares-Filho, B.S., Asner, G.P., et al., 2012. Committed carbon emissions, deforestation, and community land conversion from oil palm plantation expansion in West Kalimantan, Indonesia. Proc. Natl. Acad. Sci. 109, 7559–7564. http://dx.doi.org/10.1073/pnas.1200452109.

eCognition, 2011. eCognition Reference Book. Trimble Germany GmbH, Munich, Germany.

Cohen, W.B., Yang, Z.G., Kennedy, R., 2010. Detecting trends in forest disturbance and recovery using yearly Landsat time series: 2. TimeSync - tools for calibration and validation. Remote Sens. Environ. 114, 2911–2924. http://dx.doi.org/10.1016/j.rse.2010.07.010.

Congalton, R.G., Green, K., 2009. Assessing the accuracy of remotely sensed data: principles and practices, Second edi. CRC Press/Taylor & Francis, Boca Raton, London, New York. http://dx.doi.org/10.1111/j.1477-9730.2010.00574_2.x.

Coops, N.C., Gillanders, S.N., Wulder, M.A., Gergel, S.E., Nelson, T., Goodwin, N.R., 2010. Assessing changes in forest fragmentation following infestation using time series Landsat imagery. For. Ecol. Manag. 259, 2355–2365. http://dx.doi.org/10.1016/j.foreco.2010.03.008.

Davis, J.R., 1997. Understanding the process of decollectivisation and agricultural privatisation in transition economies: the distribution of collective and state farm assets in Latvia and Lithuania. Eur. Asia. Stud. 49, 1409–1432. http://dx.doi.org/10.1080/09668139708412507.

Deng, L., Shangguan, Z.-P., Sweeney, S., Han, F., Chen, Y., 2013. Changes in soil carbon and nitrogen following land abandonment of farmland on the Loess Plateau, China. PLoS One 8, e71923. http://dx.doi.org/10.1371/journal.pone.0071923.

Desclée, B., Bogaert, P., Defourny, P., 2006. Forest change detection by statistical object-based method. Remote Sens. Environ. 102, 1–11. http://dx.doi.org/10.1016/j.rse.2006.01.013.

DeVries, B., Decuyper, M., Verbesselt, J., Zeileis, A., Herold, M., Joseph, S., 2015. Tracking disturbance-regrowth dynamics in tropical forests using structural change detection and Landsat time series. Remote Sens. Environ. 169, 320–334. http://dx.doi.org/10.1016/j.rse.2015.08.020.

Dronova, I., Gong, P., Wang, L., 2011. Object-based analysis and change detection of major wetland cover types and their classification uncertainty during the low water period at Poyang Lake, China. Remote Sens. Environ. 115, 3220–3236. http://dx.doi.org/10.1016/j.rse.2011.07.006.

Dutrieux, L.P., Jakovac, C.C., Latifah, S.H., Kooistra, L., 2016. Reconstructing land use history from Landsat time-series: case study of a swidden agriculture system in Brazil. Int. J. Appl. Earth Obs. Geoinf. 47, 112–124. http://dx.doi.org/10.1016/j.jag.2015.11.018.

Duveiller, G., Defourny, P., 2010. A conceptual framework to define the spatial resolution requirements for agricultural monitoring using remote sensing. Remote Sens. Environ. 114, 2637–2650. http://dx.doi.org/10.1016/j.rse.2010.06.001.

Duveiller, G., Defourny, P., Desclée, B., Mayaux, P., 2008. Deforestation in Central Africa: estimates at regional, national and landscape levels by advanced processing of systematically-distributed Landsat extracts. Remote Sens. Environ. 112, 1969–1981. http://dx.doi.org/10.1016/j.rse.2007.07.026.

Espindola, G.M., Camara, G., Reis, I.A., Bins, L.S., Monteiro, A.M., 2006. Parameter selection for region-growing image segmentation algorithms using spatial autocorrelation. Int. J. Remote Sens. 27, 3035–3040. http://dx.doi.org/10.1080/01431160600617194.

Estel, S., Kuemmerle, T., Alcántara, C., Levers, C., Prishchepov, A.V., Hostert, P., 2015. Mapping farmland abandonment and recultivation across Europe using MODIS NDVI time series. Remote Sens. Environ. 163, 312–325. http://dx.doi.org/10.1016/j.rse.2015.03.028.

Evans, C., Jones, R., Svalbe, I., Berman, M., 2002. Segmenting multispectral Landsat TM images into field units. IEEE Trans. Geosci. Remote Sens. 40, 1054–1064. http://dx.doi.org/10.1109/TGRS.2002.1010893.

Exelis Visual Information Solutions, 2014. ENVI User's Guide.

FAO, 2016. FAOSTAT, Methods & standards [WWW Document]. URL. http://www.fao.org/ag/agn/nutrition/Indicatorsfiles/Agriculture.pdf (accessed 03.03.16).

García-Ruiz, J.M., Lana-Renault, N., 2011. Hydrological and erosive consequences of farmland abandonment in Europe, with special reference to the Mediterranean region – a review. Agric. Ecosyst. Environ. 140, 317–338. http://dx.doi.org/10.1016/j.agee.2011.01.003.

Gasanov, G.N., Usmanov, R.Z., Magomedov, N.R., Aitemirov, A.A., Gamidov, I.R., Adzhiev, A.M., 2013. Prevention of soil degradation and restoration of the productivity of natural pastures in the Northwestern Caspian Sea region. Arid. Ecosyst. 3, 35–38. http://dx.doi.org/10.1134/S2079096113010095.

Gellrich, M., Baur, P., Koch, B., Zimmermann, N.E., 2007. Agricultural land abandonment and natural forest re-growth in the Swiss mountains: a spatially explicit economic analysis. Agric. Ecosyst. Environ. 118, 93–108. http://dx.doi.org/10.1016/j.agee.2006.05.001.

Gibbs, H.K., Ruesch, A.S., Achard, F., Clayton, M.K., Holmgren, P., Ramankutty, N., et al., 2010. Tropical forests were the primary sources of new agricultural land in the 1980s and 1990s. Proc. Natl. Acad. Sci. 107, 16732–16737. http://dx.doi.org/10.1073/pnas.0910275107.

Gómez, C., White, J.C., Wulder, M.A., 2011. Characterizing the state and processes of change in a dynamic forest environment using hierarchical spatio-temporal segmentation. Remote Sens. Environ. 115, 1665–1679. http://dx.doi.org/10.1016/j.rse.2011.02.025.

Goulden, M.L., Mcmillan, A.M.S., Winston, G.C., Rocha, A.V., Manies, K.L., Harden, J.W., et al., 2011. Patterns of NPP, GPP, respiration, and NEP during boreal forest succession. Glob. Chang. Biol. 17, 855–871. http://dx.doi.org/10.1111/j.1365-2486.2010.02274.x.

Grogan, K., Pflugmacher, D., Hostert, P., Kennedy, R., Fensholt, R., 2015. Cross-border forest disturbance and the role of natural rubber in mainland Southeast Asia using annual Landsat time series. Remote Sens. Environ. 169, 438–453. http://dx.doi.org/10.1016/j.rse.2015.03.001.

Haddaway, N.R., Styles, D., Pullin, A.S., 2014. Environmental impacts of farm land abandonment in high altitude/mountain regions: a systematic map of the evidence. Environ. Evid. 2, 18. http://dx.doi.org/10.1186/2047-2382-2-18.

Hartvigsen, M., 2014. Land reform and land fragmentation in Central and Eastern Europe. Land Use Policy 36, 330–341. http://dx.doi.org/10.1016/j.landusepol.2013.08.016.

Huang, C., Goward, S.N., Masek, J.G., Thomas, N., Zhu, Z., Vogelmann, J.E., 2010. An automated approach for reconstructing recent forest disturbance history using dense Landsat time series stacks. Remote Sens. Environ. 114, 183–198. http://dx.doi.org/10.1016/j.rse.2009.08.017.

Ioffe, G., Nefedova, T., 2004. Marginal farmland in European Russia. Eurasian Geogr. Econ. 45, 45–59. http://dx.doi.org/10.2747/1538-7216.45.1.45.

Ioffe, G., Nefedova, T., Zaslavsky, I., 2004. From spatial continuity to fragmentation: the case of Russian farming. Ann. Assoc. Am. Geogr. 94, 913–943. http://dx.doi.org/10.1111/j.1467-8306.2004.00441.x.

Jain, M., Mondal, P., DeFries, R.S., Small, C., Galford, G.L., 2013. Mapping cropping intensity of smallholder farms: a comparison of methods using multiple sensors. Remote Sens. Environ. 134, 210–223. http://dx.doi.org/10.1016/j.rse.2013.02.029.

Jakimow, B., van der Linden, S., Hostert, P., 2017. HUB time series viewer: a concept to visualize and label remote sensing time series in QGIS. In: MultiTemp 2017. Bruges, Belgium.

Johnson, B., Xie, Z., 2011. Unsupervised image segmentation evaluation and refinement using a multi-scale approach. ISPRS J. Photogramm. Remote Sens. 66, 473–483. http://dx.doi.org/10.1016/j.isprsjprs.2011.02.006.

Keenleyside, C., Tucker, G.M., 2010. Farmland Abandonment in the EU: an Assessment of Trends and Prospects.

Kennedy, R.E., Cohen, W.B., Schroeder, T.A., 2007. Trajectory-based change detection for automated characterization of forest disturbance dynamics. Remote Sens. Environ. 110, 370–386. http://dx.doi.org/10.1016/j.rse.2007.03.010.

Kennedy, R.E., Yang, Z.G., Cohen, W.B., 2010. Detecting trends in forest disturbance and

recovery using yearly Landsat time series: 1. LandTrendr - temporal segmentation algorithms. Remote Sens. Environ. 114, 2897–2910. http://dx.doi.org/10.1016/j.rse.2010.07.008.
Kennedy, R.E., Yang, Z.Q., Cohen, W.B., Pfaff, E., Braaten, J., Nelson, P., 2012. Spatial and temporal patterns of forest disturbance and regrowth within the area of the Northwest Forest Plan. Remote Sens. Environ. 122, 117–133. http://dx.doi.org/10.1016/j.rse.2011.09.024.
Khanal, N., Watanabe, T., 2006. Abandonment of agricultural land and its consequences: a case study in the Sikles area, Gandaki Basin, Nepal Himalaya. Mt. Res. Dev. 26, 32–40. http://dx.doi.org/10.1659/0276-4741(2006)026[0032:AOALAI]2.0.CO;2.
Knoke, T., Calvas, B., Moreno, S.O., Onyekwelu, J.C., Griess, V.C., 2013. Food production and climate protection—what abandoned lands can do to preserve natural forests. Glob. Environ. Chang. 23, 1064–1072. http://dx.doi.org/10.1016/j.gloenvcha.2013.07.004.
Kraemer, R., Prishchepov, A.V., Müller, D., Kuemmerle, T., Radeloff, V.C., Dara, A., et al., 2015. Long-term agricultural land-cover change and potential for cropland expansion in the former Virgin Lands area of Kazakhstan. Environ. Res. Lett. 10, 54012. http://dx.doi.org/10.1088/1748-9326/10/5/054012.
Kuemmerle, T., Hostert, P., Radeloff, V.C., van der Linden, S., Perzanowski, K., Kruhlov, I., 2008. Cross-border comparison of post-socialist farmland abandonment in the Carpathians. Ecosystems 11, 614–628. http://dx.doi.org/10.1007/s10021-008-9146-z.
Kuemmerle, T., Müller, D., Griffiths, P., Rusu, M., 2009. Land use change in Southern Romania after the collapse of socialism. Reg. Environ. Chang. 9, 1–12. http://dx.doi.org/10.1007/s10113-008-0050-z.
Kuemmerle, T., Olofsson, P., Chaskovskyy, O., Baumann, M., Ostapowicz, K., Woodcock, C.E., et al., 2011. Post-Soviet farmland abandonment, forest recovery, and carbon sequestration in western Ukraine. Glob. Chang. Biol. 17, 1335–1349. http://dx.doi.org/10.1111/j.1365-2486.2010.02333.x.
Kuemmerle, T., Erb, K., Meyfroidt, P., Müller, D., Estel, S., Haberl, H., et al., 2013. Challenges and opportunities in mapping land use intensity globally. Curr. Opin. Environ. Sustain. 5, 484–493. http://dx.doi.org/10.1016/j.cosust.2013.06.002.
Kurganova, I., Lopes de Gerenyu, V., Six, J., Kuzyakov, Y., 2014. Carbon cost of collective farming collapse in Russia. Glob. Chang. Biol. 20, 938–947. http://dx.doi.org/10.1111/gcb.12379.
Lambin, E.F., Geist, H.J., 2006. Land use and land cover change: local processes and global impacts. In: Global Change - The IGBP Series. Springer, Berlin.
Lasanta, T., Vicente-Serrano, S.M., 2012. Complex land cover change processes in semi-arid Mediterranean regions: an approach using Landsat images in northeast Spain. Remote Sens. Environ. 124, 1–14. http://dx.doi.org/10.1016/j.rse.2012.04.023.
Lerman, Z., Csaki, C., Feder, G., 2004. Evolving farm structures and land use patterns in former socialist countries. Q. J. Int. Agric. 4, 309–335.
Lobell, D.B., Thau, D., Seifert, C., Engle, E., Little, B., 2015. A scalable satellite-based crop yield mapper. Remote Sens. Environ. 164, 324–333. http://dx.doi.org/10.1016/j.rse.2015.04.021.
Loboda, T., Krankina, O., Savin, I., Kurbanov, E., Hall, J., 2017. Land management and the impact of the 2010 extreme drought event on the agricultural and ecological systems of European Russia. In: Land-Cover and Land-Use Changes in Eastern Europe after the Collapse of the Soviet Union in 1991. Springer International Publishing, Cham, pp. 173–192. http://dx.doi.org/10.1007/978-3-319-42638-9_8.
Loveland, T.R., Dwyer, J.L., 2012. Landsat: building a strong future. Remote Sens. Environ. 122, 22–29. http://dx.doi.org/10.1016/j.rse.2011.09.022.
Marceau, D.J., 1999. The scale issue in the social and natural sciences. Can. J. Remote. Sens. 25, 347–356. http://dx.doi.org/10.1080/07038992.1999.10874734.
Markwardt, C.B., 2009. Non-linear Least-squares Fitting in IDL with MPFIT. In: Astron. Data Anal. Softw. Syst. XVIII ASP Conf. Ser. 411. 251 (doi:citeulike-article-id:4067445).
Masek, J.G., Vermote, E.F., Saleous, N.E., Wolfe, R., Hall, F.G., Huemmrich, K.F., et al., 2006. A Landsat surface reflectance dataset for North America, 1990–2000. Geosci. Remote Sens. Lett. IEEE 3, 68–72. http://dx.doi.org/10.1109/LGRS.2005.857030.
Meyer, W.B., Turner, B.L., 1992. Human-population growth and global land-use cover change. Annu. Rev. Ecol. Syst. 23, 39–61.
Meyfroidt, P., Schierhorn, F., Prishchepov, A.V., Müller, D., Kuemmerle, T., 2016. Drivers, constraints and trade-offs associated with recultivating abandoned cropland in Russia, Ukraine and Kazakhstan. Glob. Environ. Chang. 37, 1–15. http://dx.doi.org/10.1016/j.gloenvcha.2016.01.003.
Müller, D., Munroe, D., 2008. Changing rural landscapes in Albania: cropland abandonment and forest clearing in the postsocialist transition. Ann. Assoc. Am. Geogr. 98, 855–876. http://dx.doi.org/10.1080/00045600802262323.
Müller, D., Kuemmerle, T., Rusu, M., Griffiths, P., 2009. Lost in transition: determinants of post-socialist cropland abandonment in Romania. J. Land Use Sci. 4, 109–129. http://dx.doi.org/10.1080/17474230802645881.
Navarro, L.M., Pereira, H.M., 2015. Rewilding abandoned landscapes in Europe. In: Rewilding European Landscapes, pp. 3–23. http://dx.doi.org/10.1007/978-3-319-12039-3_1.
O'Loughlin, J., Witmer, F.D.W., 2011. The localized geographies of violence in the North Caucasus of Russia, 1999–2007. Ann. Assoc. Am. Geogr. 101, 178–201. http://dx.doi.org/10.1080/00045608.2010.534713.
Obrist, M.K., Rathey, E., Bontadina, F., Martinoli, A., Conedera, M., Christe, P., et al., 2011. Response of bat species to sylvo-pastoral abandonment. For. Ecol. Manag. 261, 789–798. http://dx.doi.org/10.1016/j.foreco.2010.12.010.
Olofsson, P., Foody, G.M., Herold, M., Stehman, S.V., Woodcock, C.E., Wulder, M.A., 2014. Good practices for estimating area and assessing accuracy of land change. Remote Sens. Environ. 148, 42–57. http://dx.doi.org/10.1016/j.rse.2014.02.015.
Ozdogan, M., Woodcock, C.E., 2006. Resolution dependent errors in remote sensing of cultivated areas. Remote Sens. Environ. 103, 203–217. http://dx.doi.org/10.1016/j.rse.2006.04.004.
Plieninger, T., Hui, C., Gaertner, M., Huntsinger, L., Smith, P., Gregory, P., et al., 2014. The impact of land abandonment on species richness and abundance in the Mediterranean basin: a meta-analysis. PLoS One 9, e98355. http://dx.doi.org/10.1371/journal.pone.0098355.
Pointereau, P., Coulon, F., Girard, P., L., M., Stuczynski, T., Ortega, V.S., del Rio, A., 2008. Analysis of farmland abandonment and the extent and location of agricultural areas that are actually abandoned or are in risk to be abandoned. In: Anguiano, E., Bamps, C., Terres, J.-M. (Eds.), JRC Scientific and Technical Reports (EUR 23411 EN).
Prishchepov, A.V., Radeloff, V.C., Baumann, M., Kuemmerle, T., Müller, D., 2012. Effects of institutional changes on land use: agricultural land abandonment during the transition from state-command to market-driven economies in post-Soviet Eastern Europe. Environ. Res. Lett. 7, 24021. http://dx.doi.org/10.1088/1748-9326/7/2/024021.
Prishchepov, A.V., Müller, D., Baumann, M., Kuemmerle, T., Alcántara, C., Radeloff, V.C., 2017. Underlying drivers and spatial determinants of post-Soviet agricultural land abandonment in temperate Eastern Europe. In: Land-Cover and Land-Use Changes in Eastern Europe after the Collapse of the Soviet Union in 1991. Springer International Publishing, Cham, pp. 91–117. http://dx.doi.org/10.1007/978-3-319-42638-9_5.
Pu, R., Landry, S., Yu, Q., 2011. Object-based urban detailed land cover classification with high spatial resolution IKONOS imagery. Int. J. Remote Sens. 32, 3285–3308. http://dx.doi.org/10.1080/01431161003745657.
R Core Team, 2016. R: A language and environment for statistical computing. R Foundation for Statistical Computing, Vienna, Austria.
Ramankutty, N., Foley, J.A., 1999. Estimating historical changes in global land cover: croplands from 1700 to 1992. Glob. Biogeochem. Cycles 13, 997–1027. http://dx.doi.org/10.1029/1999gb900046.
Renwick, A., Jansson, T., Verburg, P.H., Revoredo-Giha, C., Britz, W., Gocht, A., et al., 2013. Policy reform and agricultural land abandonment in the EU. Land Use Policy 30, 446–457. http://dx.doi.org/10.1016/j.landusepol.2012.04.005.
ROSSTAT, 2010. Vserossiyskoy perepis' naseleniya 2010 goda. 3. Naseleniye po natsional'nosti i vladen iyu Russkim yazykom po sub'yektam. (All-Russian Census of Population 2010. 3. Population by Nationality and Command of the Russian Language by Federation Subjects).
ROSSTAT, 2016. Central Statistical Database. Federal Service of State Statistics of the Russian Federation.
Rudorff, B.F.T., Batista, G.T., 1991. Wheat yield estimation at the farm level using TM Landsat and agrometeorological data. Int. J. Remote Sens. 12, 2477–2484. http://dx.doi.org/10.1080/01431169108955281.
Saraykin, V., Yanbykh, R., Uzun, V., 2017. Assessing the potential for Russian grain exports: a special focus on the prospective cultivation of abandoned land. In: The Eurasian Wheat Belt and Food Security. Springer International Publishing, Cham, pp. 155–175. http://dx.doi.org/10.1007/978-3-319-33239-0_10.
Schierhorn, F., Müller, D., Beringer, T., Prishchepov, A.V., Kuemmerle, T., Balmann, A., 2013. Post-Soviet cropland abandonment and carbon sequestration in European Russia, Ukraine, and Belarus. Glob. Biogeochem. Cycles 27, 1175–1185. http://dx.doi.org/10.1002/2013GB004654.
Schmidt, M., Pringle, M., Devadas, R., Denham, R., Tindall, D., 2016. A framework for large-area mapping of past and present cropping activity using seasonal landsat images and time series metrics. Remote Sens. 8. http://dx.doi.org/10.3390/rs8040312.
Schultz, B., Immitzer, M., Formaggio, A.R., Sanches, I.D.A., Luiz, A.J.B., Atzberger, C., 2015. Self-guided segmentation and classification of multi-temporal Landsat 8 images for crop type mapping in Southeastern Brazil. Remote Sens. 7, 14482–14508. http://dx.doi.org/10.3390/rs71114482.
Shagaida, N., Svetlov, N.M., Uzun, V.Y., Loginova, D.A., Prishchepov, A.V., 2017. Potential of Growth of Agricultural Production in Russia at the Expense of Recultivation of Abandoned Agricultural Lands (Potencial Rosta Sel'skohozjajstvennogo Proizvodstva Rossii Za Schjot Vovlechenija v Oborot Neispol'zuemyh Sel'skohozjajstvennyh Ug).
Sieber, A., Uvarov, N.V., Baskin, L.M., Radeloff, V.C., Bateman, B.L., Pankov, A.B., et al., 2015. Post-Soviet land-use change effects on large mammals' habitat in European Russia. Biol. Conserv. 191, 567–576. http://dx.doi.org/10.1016/j.biocon.2015.07.041.
Smaliychuk, A., Müller, D., Prishchepov, A.V., Levers, C., Kruhlov, I., Kuemmerle, T., 2016. Recultivation of abandoned agricultural lands in Ukraine: patterns and drivers. Glob. Environ. Chang. 38, 70–81. http://dx.doi.org/10.1016/j.gloenvcha.2016.02.009.
Stehman, S.V., 2014. Estimating area and map accuracy for stratified random sampling when the strata are different from the map classes. Int. J. Remote Sens. 35, 4923–4939. http://dx.doi.org/10.1080/01431161.2014.930207.
Stehman, S.V., Wickham, J., Smith, J.H., Yang, L., 2003. Thematic accuracy of the 1992 National Land-Cover Data for the eastern United States: statistical methodology and regional results. Remote Sens. Environ. 86, 500–516. http://dx.doi.org/10.1016/S0034-4257(03)00128-7.
Swinnen, J., Burkitbayeva, S., Schierhorn, F., Prishchepov, A.V., Müller, D., 2017. Production potential in the "bread baskets" of Eastern Europe and Central Asia. Glob. Food Sec. http://dx.doi.org/10.1016/j.gfs.2017.03.005.
Uzun, V., Saraikin, V., Gataulina, E., Shagaida, N., Yanbykh, R., Mary, S., et al., 2014. Prospects of the Farming Sector and Rural Development in View of Food Security: The Case of the Russian Federation.
Van Eetvelde, V., Antrop, M., 2004. Analyzing structural and functional changes of traditional landscapes - two examples from Southern France. Landsc. Urban Plan. 67, 79–95. http://dx.doi.org/10.1016/S0169-2046(03)00030-6.
Verbesselt, J., Hyndman, R., Newnham, G., Culvenor, D., 2010. Detecting trend and seasonal changes in satellite image time series. Remote Sens. Environ. 114, 106–115.

http://dx.doi.org/10.1016/j.rse.2009.08.014.
Vieira, M.A., Formaggio, A.R., Rennó, C.D., Atzberger, C., Aguiar, D.A., Mello, M.P., 2012. Object based image analysis and data mining applied to a remotely sensed Landsat time-series to map sugarcane over large areas. Remote Sens. Environ. 123, 553–562. http://dx.doi.org/10.1016/j.rse.2012.04.011.
Vrieling, A., Skidmore, A.K., Wang, T., Meroni, M., Ens, B.J., Oosterbeek, K., et al., 2017. Spatially detailed retrievals of spring phenology from single-season high-resolution image time series. Int. J. Appl. Earth Obs. Geoinf. 59, 19–30. http://dx.doi.org/10.1016/j.jag.2017.02.021.
Wulder, M.A., Masek, J.G., Cohen, W.B., Loveland, T.R., Woodcock, C.E., 2012. Opening the archive: how free data has enabled the science and monitoring promise of Landsat. Remote Sens. Environ. 122, 2–10. http://dx.doi.org/10.1016/j.rse.2012.01.010.
Xian, G., Homer, C., Fry, J., 2009. Updating the 2001 National Land Cover Database land cover classification to 2006 by using Landsat imagery change detection methods. Remote Sens. Environ. 113, 1133–1147. http://dx.doi.org/10.1016/j.rse.2009.02.004.
Xie, Y., Weng, Q., 2016. Updating urban extents with nighttime light imagery by using an object-based thresholding method. Remote Sens. Environ. 187, 1–13. http://dx.doi.org/10.1016/j.rse.2016.10.002.
Yan, L., Roy, D.P., 2014. Automated crop field extraction from multi-temporal web enabled Landsat data. Remote Sens. Environ. 144, 42–64. http://dx.doi.org/10.1016/j.rse.2014.01.006.
Yan, L., Roy, D.P., 2015. Improved time series land cover classification by missing-observation-adaptive nonlinear dimensionality reduction. Remote Sens. Environ. 158, 478–491. http://dx.doi.org/10.1016/j.rse.2014.11.024.
Yan, L., Roy, D.P., 2016. Conterminous United States crop field size quantification from multi-temporal Landsat data. Remote Sens. Environ. 172, 67–86. http://dx.doi.org/10.1016/j.rse.2015.10.034.
Yin, H., Khamzina, A., Pflugmacher, D., Martius, C., 2017. Forest cover mapping in post-Soviet Central Asia using multi-resolution remote sensing imagery. Sci. Rep. 7, 1375.
Yu, W., Zhou, W., Qian, Y., Yan, J., 2016. A new approach for land cover classification and change analysis: integrating backdating and an object-based method. Remote Sens. Environ. 177, 37–47. http://dx.doi.org/10.1016/j.rse.2016.02.030.
Zheng, B., Myint, S.W., Thenkabail, P.S., Aggarwal, R.M., 2015. A support vector machine to identify irrigated crop types using time-series Landsat NDVI data. Int. J. Appl. Earth Obs. Geoinf. 34, 103–112. http://dx.doi.org/10.1016/j.jag.2014.07.002.
Zhu, Z., Woodcock, C.E., 2012. Object-based cloud and cloud shadow detection in Landsat imagery. Remote Sens. Environ. 118, 83–94. http://dx.doi.org/10.1016/j.rse.2011.10.028.
Zhu, Z., Woodcock, C.E., 2014. Continuous change detection and classification of land cover using all available Landsat data. Remote Sens. Environ. 144, 152–171. http://dx.doi.org/10.1016/j.rse.2014.01.011.